To: Dr. Lucia Tsaoussi

From: David Tobin, Chris Moeller, Robert Holz
University of Wisconsin-Madison, Space Science and Engineering Center

Date: 11 February 2013

Re: **Year 1 Progress Report for NASA Award Number NNX12AG68G, Hyperspectral Infrared Satellite Intercalibration Studies,**

1. Summary

This is the year 1 progress report for NASA Award Number NNX12AG68G, "Hyperspectral Infrared Satellite Intercalibration Studies", selected as part of the NASA Research Announcement "Satellite Calibration Interconsistency Studies" (SICS11) (solicitation NNH11ZDA001N-SCIS).

The objectives of our work were described in the proposal and are summarized here again. Combining with our previous intercalibration efforts and extending the satellite record further, the overall objectives of this work are:

1) To perform intercalibration studies of the High Spectral Resolution (HSR) infrared sounder observations (including AIRS, IASI on METOP-A and METOP-B, and CrIS) to achieve a new level of absolute accuracy and consistency for improved weather forecasting and climate studies, and
2) To use the HSR datasets to assess and improve the calibration of the collocated Narrow Band (NB) imagers (including MODIS on Terra and Aqua, VIIRS on NPP, and AVHRR on METOP-A and B).

Components of both objectives include collecting the required data and conducting the intercomparisons, analyzing the results to understand and characterize the calibration biases and quantify the calibration uncertainties of each sensor, where possible making refinements to the sensor calibration algorithms or calibration coefficients to improve the calibrations, and finally to work with radiance and retrieval product communities to make optimal use of our findings.

Table 1 shows all of the various intercalibration studies pursued under this project. A version of this table was included in the proposal to indicate the priority and intercalibration method (Simultaneous Nadir Overpass (SNO), Same Satellite, and Tandem) of each case, as well as intercomparisons for which we have previous results highlighted with black boxes and "*". Here it is used to highlight, with purple boxes, the analyses that are reported in this report. These include the CrIS/AIRS, CrIS/IASI, CrIS/VIIRS, and IASI/VIIRS intercalibrations. As proposed, our first year efforts have focused on the comparison of high spectral resolution sensors CrIS/IASI/AIRS, as well as a focus on CrIS and VIIRS given the launch of Suomi-NPP in late 2011. Two papers have been written to provide summaries of these efforts:

- *Tobin et al., 2012, Cross-track Infrared Sounder (CrIS) Spectral Radiance Calibration and Evaluations, American Institute of Physics, in Proceedings of the 2012 International Radiation Symposium, in press.*

- *Tobin et al., 2013, Suomi NPP/JPSS Cross-track Infrared Sounder (CRIS): Intercalibration with AIRS, IASI, AND VIIRS, AMS Annual Meeting, Austin, TX, January 2013.*

The reminder of the report includes detailed results for each of these intercalibration studies. In general, we have accomplished a lot of work in this first year. We look forward to any feedback on the results presented below or path forward.

	Aqua AIRS	METOP-A IASI	METOP-B IASI	NPP CrIS	Aqua MODIS	Terra MODIS	NPP VIIRS	METOP-A AVHRR	METOP-B AVHRR
Aqua AIRS		SNO*	SNO	Tandem	Same Satellite*	SNO	Tandem	SNO	SNO
METOP-A IASI			Tandem	SNO	SNO*	Tandem*	SNO	Same Satellite*	Tandem
METOP-B IASI				SNO	SNO	Tandem	SNO	Tandem	Same Satellite
NPP CrIS					Tandem	SNO	Same Satellite	SNO	SNO
Aqua MODIS						X	X	X	X
Terra MODIS							X	X	X
NPP VIIRS								X	X
METOP-A AVHRR									X
METOP-B AVHRR									

Table 1. Summary of the various sensor intercalibration studies of this project, per the proposal. Black boxes denote studies for which we have previous results and purple boxes denote studies that are included in this year 1 report.

2. CRIS/AIRS INTERCOMPARISON RESULTS

CrIS/AIRS comparisons have been very useful in the first year of Suomi-NPP due to the large yield due to the similar orbits of Suomi-NPP and Aqua, and because a large number of validation studies have been performed to date on the AIRS data making it a known quantity for evaluating the more recent CrIS data. The AIRS/CrIS intercomparison method and sample results are presented using Figures 2.1 through 2.7.

The intercomparison technique involves collecting the CrIS and AIRS data found within 100km of the Simultaneous Nadir Overpass (SNO) locations that occur with +/- 20 minute simultaneity. A sample of this is shown on the left hand side of Figure 2.1. For each such case, the mean and standard deviation of the radiance spectra are recorded for both CrIS and AIRS. The right hand side of Figure 2.1 shows an important result: for large ensembles of SNOs the spatial collocation errors of this approach are random and gaussianly distributed, according the spatial

variability of the scenes, and unbiased. The full distribution for all scenes is the sum of many gaussians. This leads to a simple yet powerful and accurate method for computing biases between the two sensors where a weighted mean difference between the two sensors is computed, using the spatial variability of each SNO to provide the weights. The uncertainty in the weighted mean differences is also computed. This is done independently for each spectral channel after performing spectral manipulations to account (as much as possible) for the differences in the spectral responses of CrIS and AIRS.

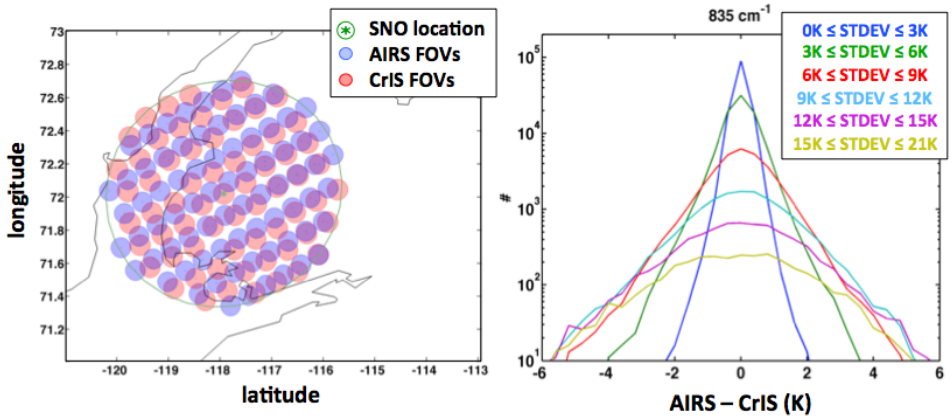

Figure 2.1. A sample CrIS/AIRS SNO (left hand side) and the distribution of 835 cm-1 brightness temperature differences for various ranges of spatial variability for a large ensemble of SNOs.

Because Suomi-NPP and EOS Aqua are in similar orbits, there are many SNOs distributed over a wide range of latitude and longitude. Collocations collected between 25 Feb and 18 Dec 2012 are shown in Figure 2.2. This includes "SNOs" for view angles less than or equal to 30 degrees and CrIS/AIRS view angle differences less than 3 degrees (i.e. not just pure nadir cases). AIRS data is L1B v5 and CrIS data is calibrated using ADL/CSPP v1.1 with native engineering packet contents.

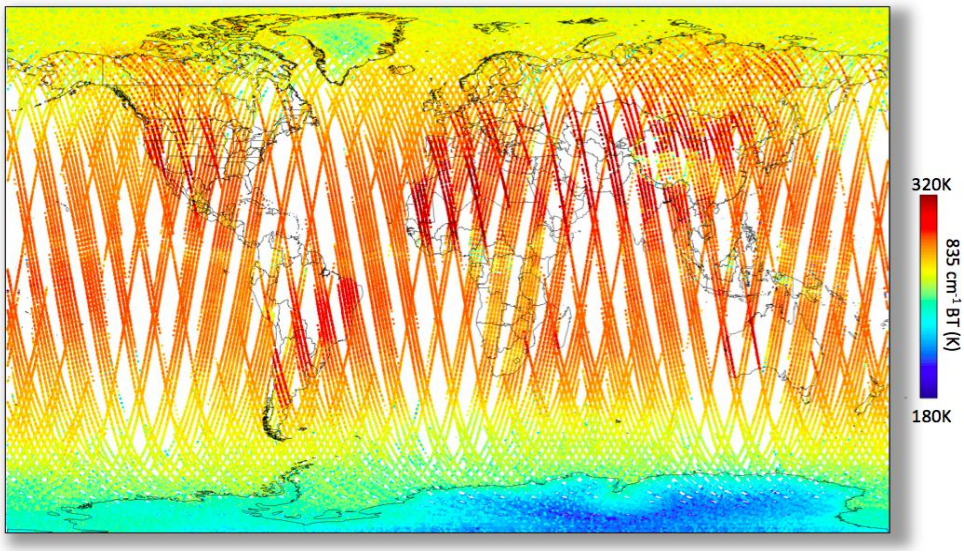

Figure 2.2. The spatial map of 598,083 CrIS/AIRS SNOs collected between 25 Feb to 18 Dec 2012. Scan angles ≤ 30°; Scan angle difference ≤ 3°; Time Diff <= 20 min. AIRS data is L1B v5; CrIS data is ADL (CSPP v1.1) with native Eng. Packets.

Due to the imprecise methodology for normalizing the spectral response functions of CrIS and AIRS, and due to the time dependent variations in the AIRS spectral calibration, the comparisons shown here are limited to 10 wavenumber averages. This averaging minimizes these issues and produces a more meaningful assessment of the radiometric differences between CrIS and AIRS. The sample wavenumber regions chosen are shown in Figure 2.3. These regions include opaque and more transparent regions of each spectral band of CrIS, and include sensitivity to various components of the CrIS radiometric calibration. For example, the longwave CO_2 region is most sensitive to the longwave band nonlinearity correction while the longwave window is most sensitive to the CrIS Internal Calibration Target (ICT) temperature. Similarly the 1590 cm^{-1} and 2500 cm^{-1} regions have sensitivity to the CrIS ICT environmental model. AIRS, of course, also has sensitivity to its own calibration issues as well.

Using this approach and data, sample results are shown in Figures 2.4 through 2.7. These sample results show that the radiometric agreement between CrIS and AIRS is very good – less than ~0.1K (Figure 2.5). The differences are also very stable with time (Figure 2.6), and do not show large dependence on scene brightness temperature (Figure 2.7).

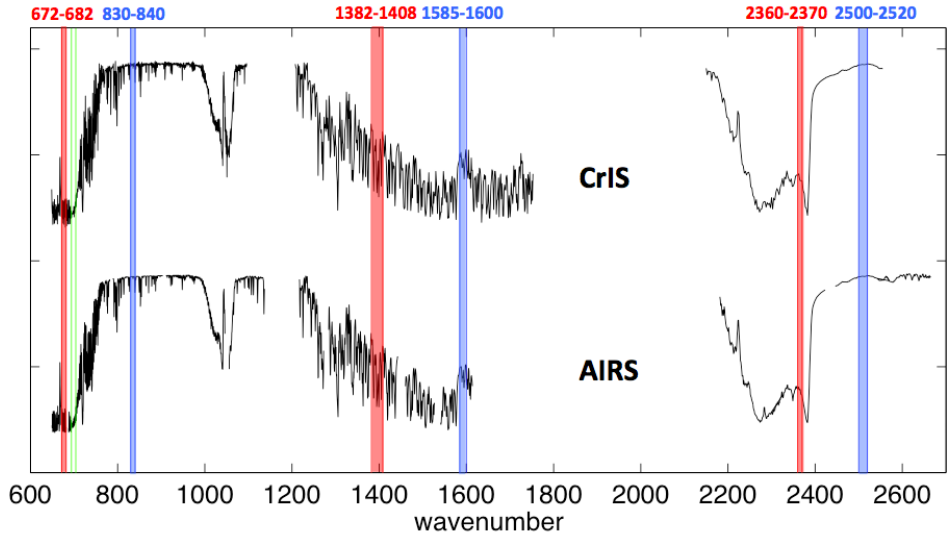

Figure 2.3. Sample CrIS and AIRS brightness temperature spectra and sample, representative wavenumber regions for the comparisons shown in Figures 2.4 through 2.7.

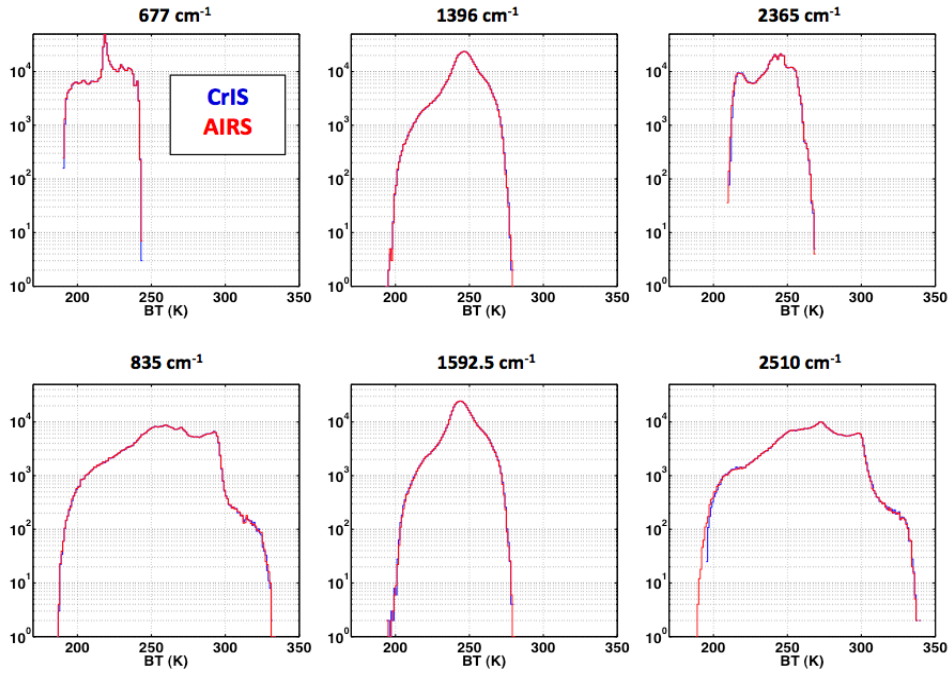

Figure 2.4. Log-scale brightness temperature distributions of CrIS and AIRS for the wavenumber regions shown in Figure 2.3.

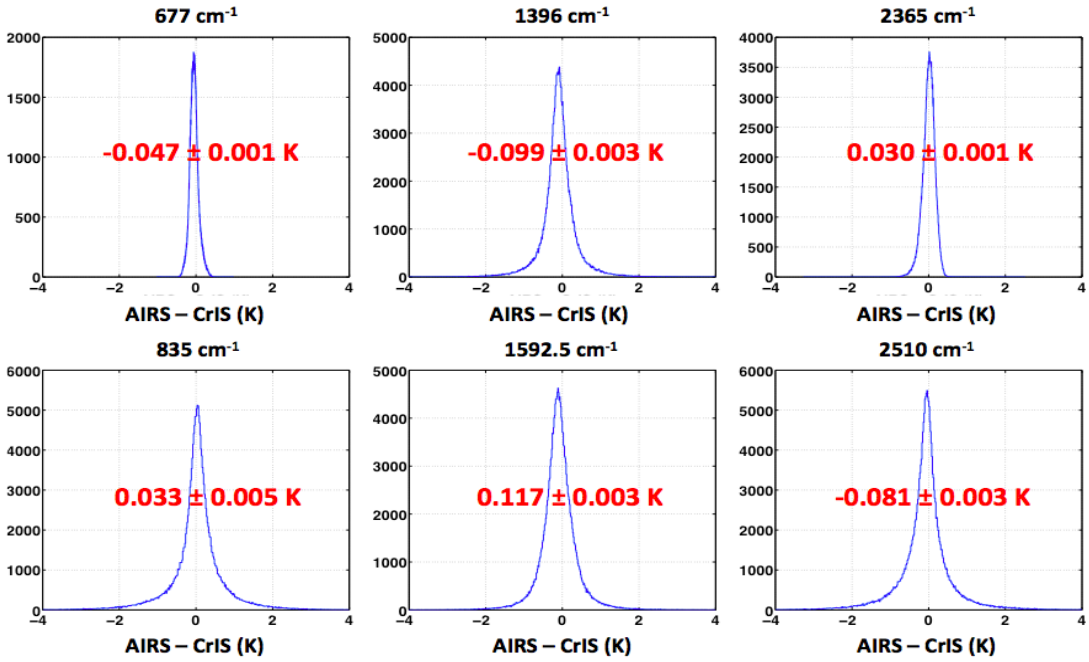

Figure 2.5. Distributions of brightness temperature differences, with mean differences and uncertainties in the mean listed in red.

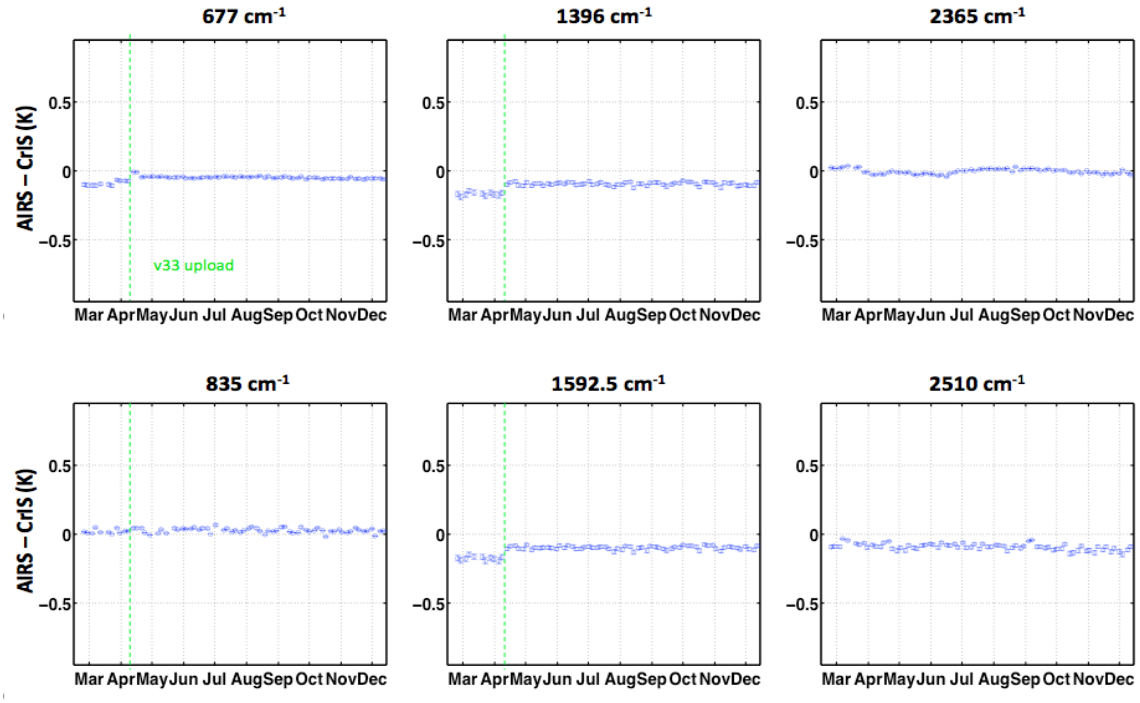

Figure 2.6. Time series of differences. The discontinuity in mid April is due to an update in the CrIS calibration coefficients at that time.

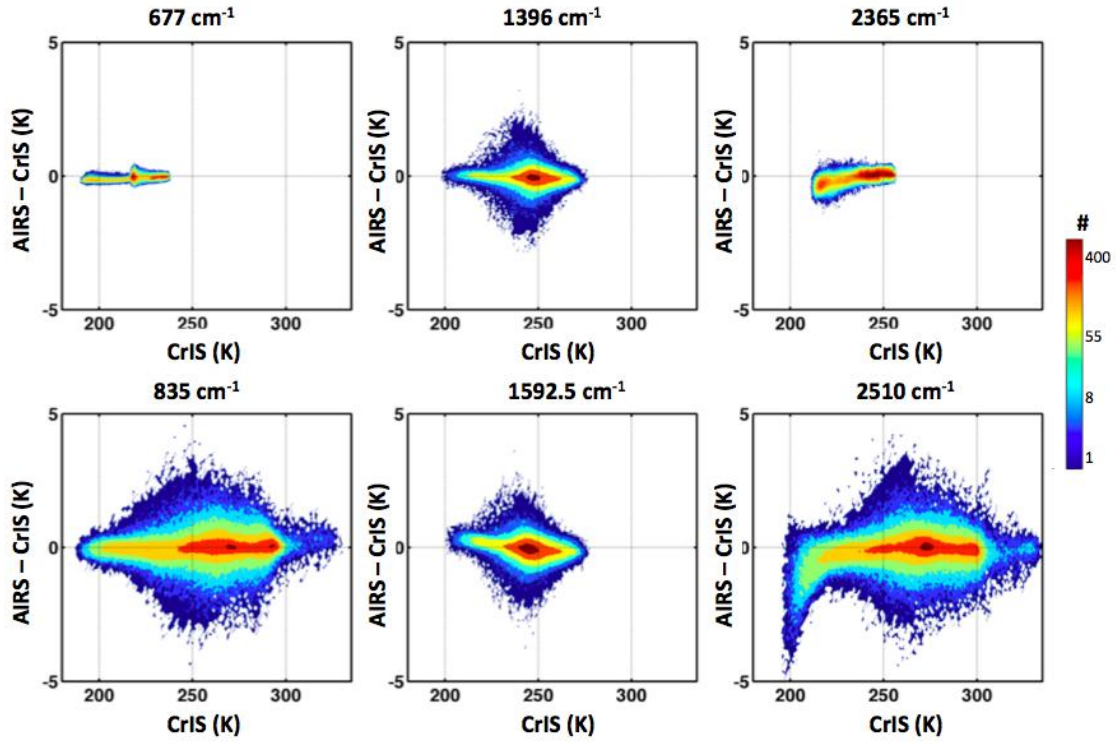

Figure 2.7. Log-scale distributions of brightness temperature differences as a function of scene brightness temperature. Dark blue is one count (one SNO) and dark red is 400.

3. CRIS/IASI INTERCOMPARISON RESULTS

The same basic methodology described for comparing CrIS and AIRS is also used for comparing CrIS and IASI. However, due to different orbits, the CrIS/IASI collocations only occur at high latitudes, and here only nadir cases are included. Additionally, because the spectral resolution differences of CrIS and IASI can be rigorously accounted for, the comparisons are shown here for the complete spectrum of CrIS. These comparisons are therefore sensitive to both the radiometric and spectral characteristics of CrIS (and IASI).

The latitude and time dependence of the CrIS/IASI SNOs are shown in Figure 3.1. The SNOs occur at latitudes of +/- 72.4 degrees. For time simultaneity of +/- 20 minutes the SNOs occur for periods of ~20 days separated by ~30 day gaps. The ensemble used here includes 2203 cases collected between March and November of 2012.

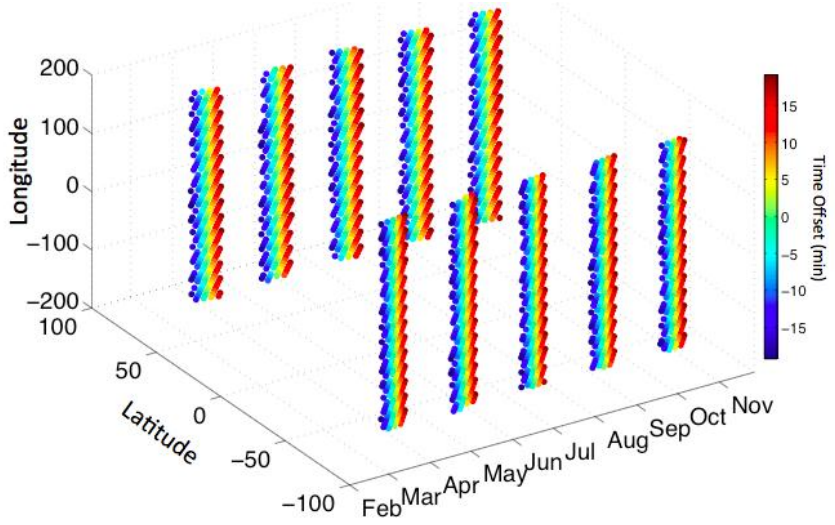

Figure 3.1. Latitude and time dependence of the CrIS/IASI SNOs.

Using this ensemble of SNOs, the mean differences and uncertainties are shown in Figures 3.2 and 3.3 for the Northern and Southern SNOs, respectively. The overall agreement between CrIS and IASI is very good – less than a few tenth K for the large majority of channels. These comparisons use a Hamming apodization to suppress a known artifact in the current CrIS products – additional spectral (Gibbs effect) ringing in the CrIS spectra. This is a topic of current investigation of the CrIS Cal/Val team. Additionally, larger deviations are seen between CrIS and IASI for very cold scene temperatures in portions of the shortwave spectral band. These artifacts are also seen in comparisons with AIRS and in clear sky obs-calcs, and is also a topic of current investigation by the Cal/Val team.

Lastly, the FOV dependence of the CrIS/IASI differences is shown in Figure 3.4. The FOV dependence of the differences is very small – significantly less than 0.1K for the majority of spectral channels.

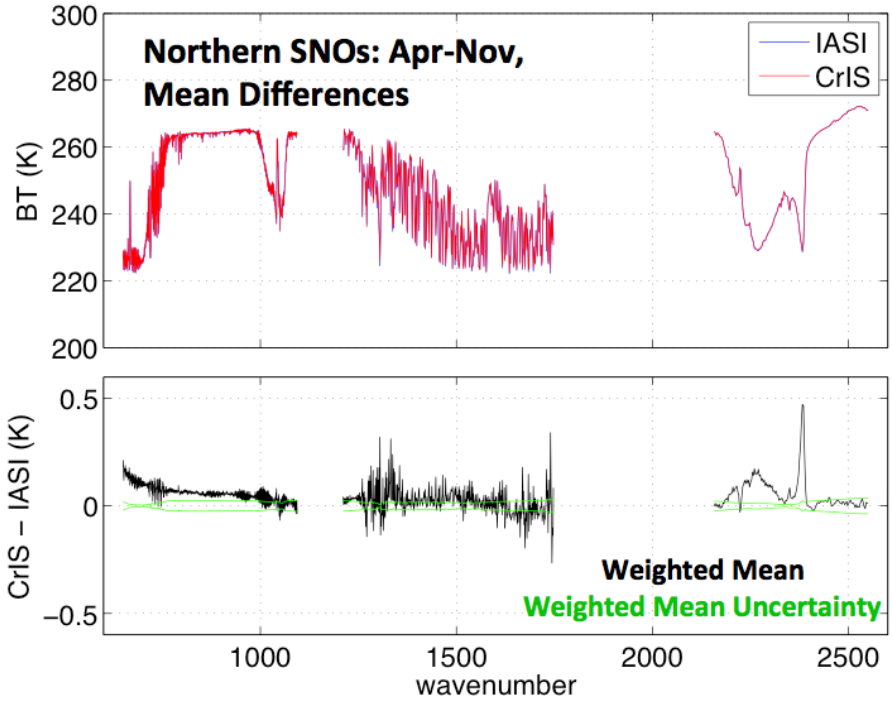

Figure 3.2. Mean spectra, weighted mean differences, and uncertainties for Northern CrIS/IASI SNOs.

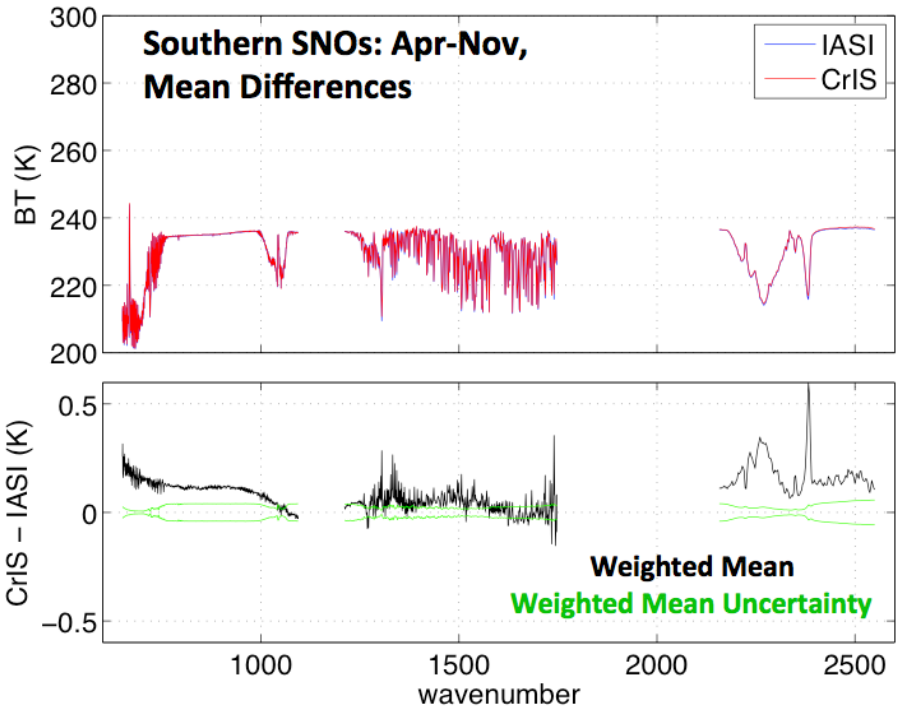

Figure 3.3. Same as Figure 3.2 but for Southern CrIS/IASI SNOs.

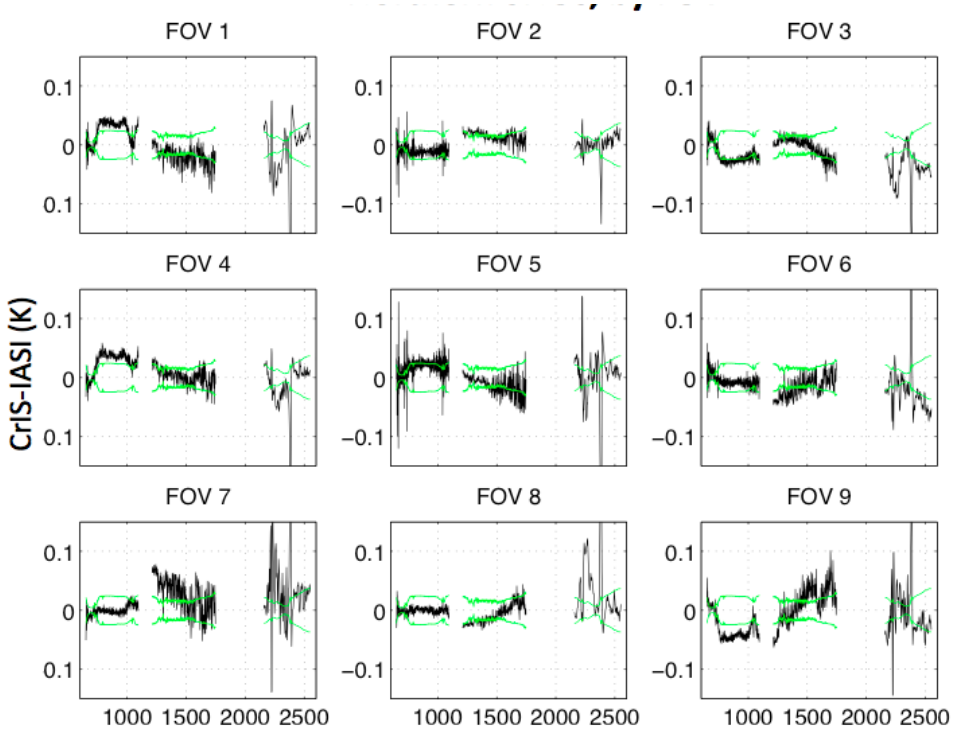

Figure 3.4. Northern CrIS/IASI SNO differences (weighted mean difference in black; weighted mean difference uncertainty in green) for each CrIS FOV.

4. CRIS/VIIRS INTERCOMPARISON RESULTS

Analogous to our previous comparisons of AIRS and MODIS on EOS Aqua, here we present results of intercomparing CrIS and VIIRS on Suomi-NPP. A sample CrIS spectrum and the VIIRS Spectral Response Functions (SRFs) are shown in Figure 3.1. Using VIIRS bands where CrIS provides spectral coverage, the comparisons are computed for VIIRS bands M13 (4μm), M15 (10.8μm), and M16 (12μm). It should be noted, however, that VIIRS bands M15 and M16 SRFs include an out-of-band (OOB) contribution in the gap in the CrIS spectra at ~9□m.

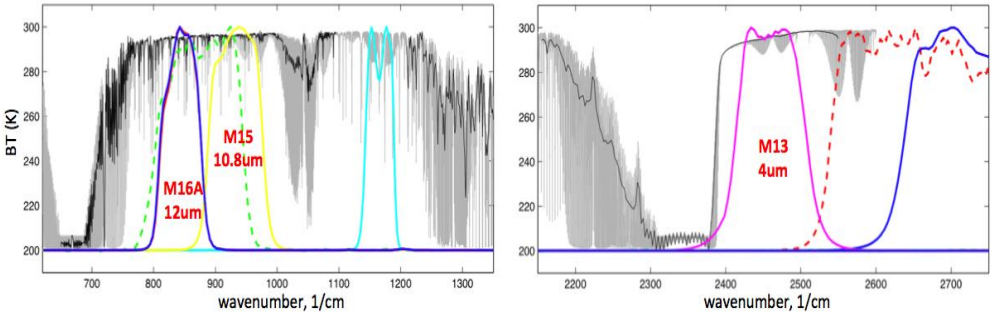

Figure 3.1. Sample monochromatic (grey) and CrIS spectra (black) overlaid with VIIRS SRFs.

Comparisons of CrIS and VIIRS are performed by, for each CrIS footprint/spectrum, convolving the CrIS spectrum with the VIIRS SRFs and computing the mean VIIRS radiances (and standard deviation) with the CrIS footprint. Spatially uniform scenes are then selected and differences between CrIS and VIIRS are computed. A sample set of data for descending node

data for VIIRS M15 is shown in Figure 3.2. This results in approximately 500,000 collocated footprints suitable for comparison every day.

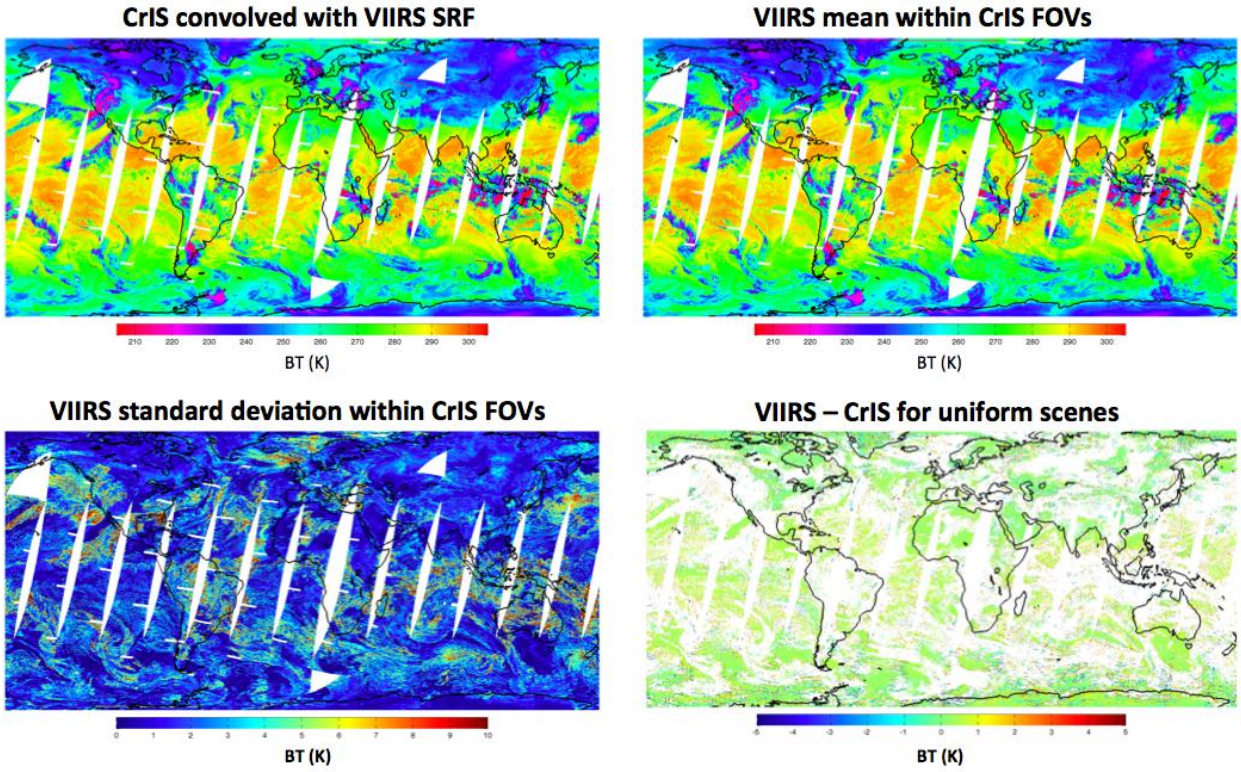

Figure 3.2. Sample comparisons of CrIS and VIIRS M15 for nighttime data on 25 February 2012.

Using this data, sample results are shown in Figures 3.3 through 3.6. Figure 3.3 shows the time dependence of daily mean differences. The mean differences are less than 0.1K and are very stable with time. Larger deviations in the March/April time frame are due to sensor/calibration changes at that time. VIIRS nonlinearity tests, performed quarterly, are evident in the time series.

Figure 3.4 shows the scene temperature dependence of the CrIS/VIIRS differences. Bands M13 and M16 show little (less than ~0.1K) dependence on scene temperature while band M15 shows are stronger dependence on scene temperatures, with differences approaching -0.4K for scenes at 200K. A small portion of this difference could be due to the VIIRS OOB SRF. It is very unlikely that CrIS could have significantly different scene temperature dependence between 12□m (M16) and 10.8□m (M15). These differences are under investigation by both the CrIS and VIIRS teams.

The scan angle dependence of the CrIS/VIIRS differences is shown in Figure 3.5. This dependence is very small.

Finally, the time dependence of the CrIS/VIIRS differences during one of the VIIRS nonlinearity characterization tests is shown in Figure 3.6. During this test, the VIIRS calibration blackbody (OBC) temperature is allowed to cool from a nominal value of ~292K to below 270K. When this occurs, the agreement between the three VIIRS bands improves, and the agreement between CrIS and VIIRS improves. This general behavior is also seen for the other on-board nonlinearity tests. This implies that further improvement in the VIIRS calibration is possible, with refinements to the OBC temperature and/or background instrument temperatures. Note the period nature of

the larger M15 band differences; this is due colder scene temperatures at the pole crossings as discussed with Figure 3.4.

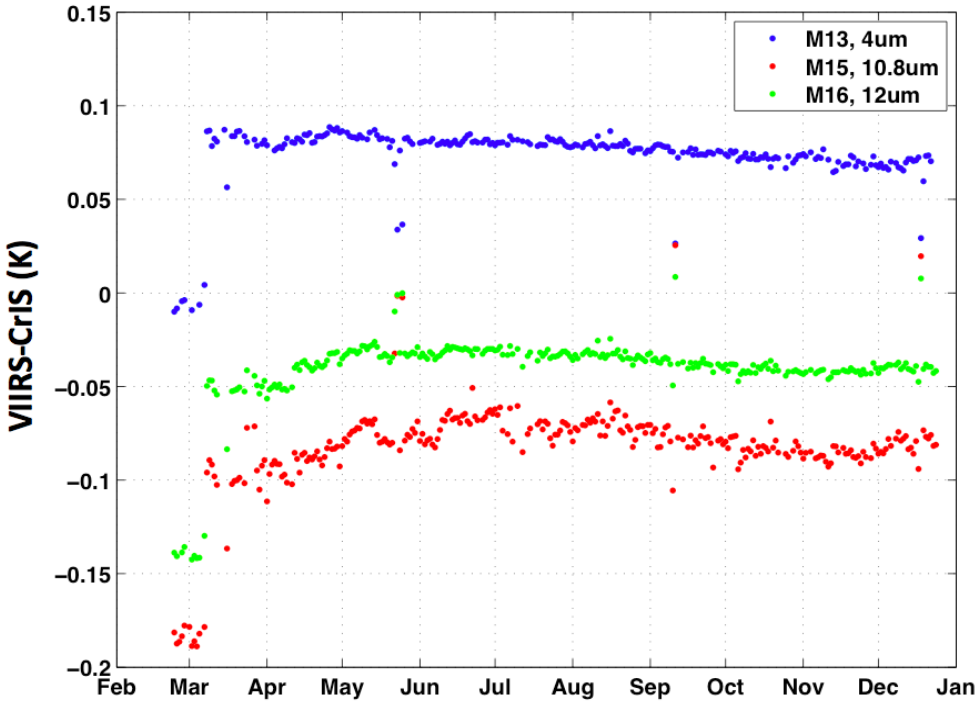

Figure 3.3. Time dependence of daily mean CrIS/VIIRS differences.

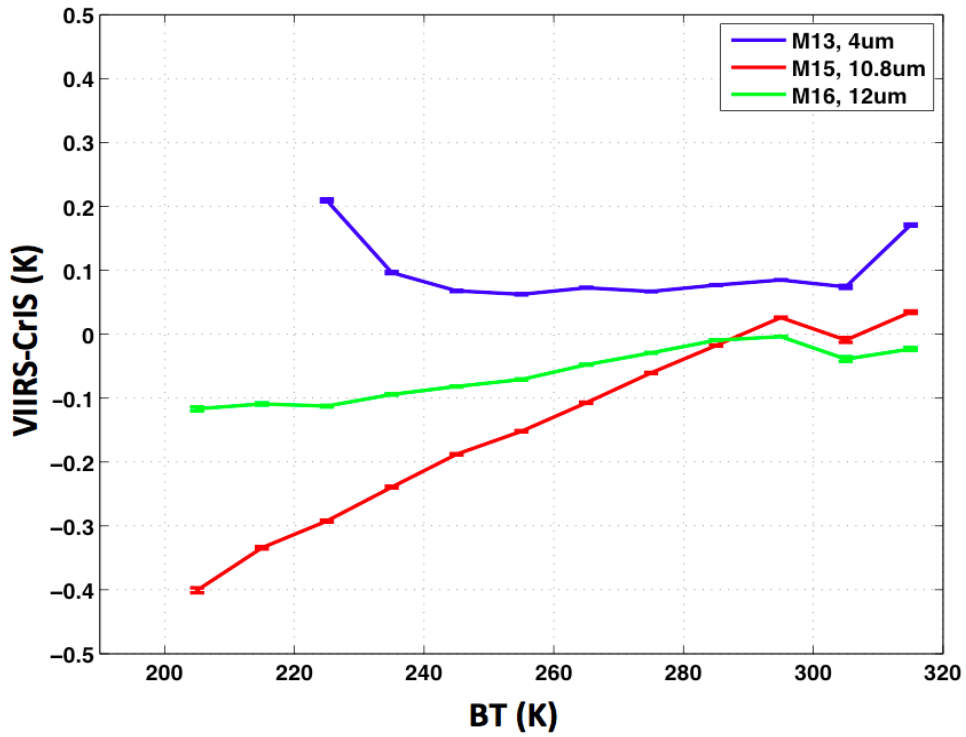

Figure 3.4. Scene temperature dependence of the CrIS/VIIRS differences.

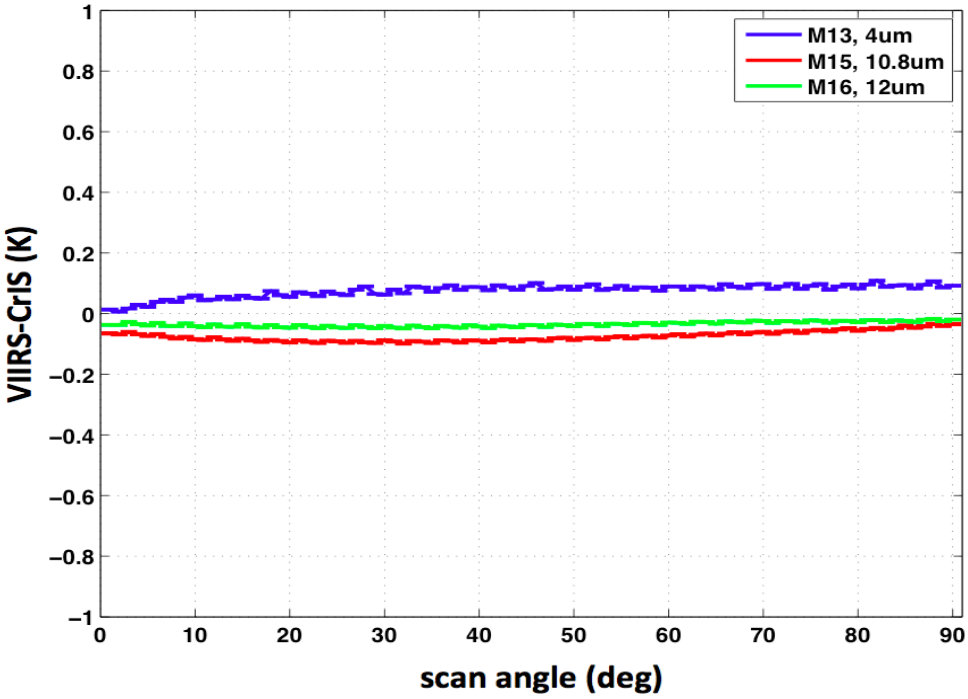

Figure 3.5. Scan angle dependence of the CrIS/VIIRS differences.

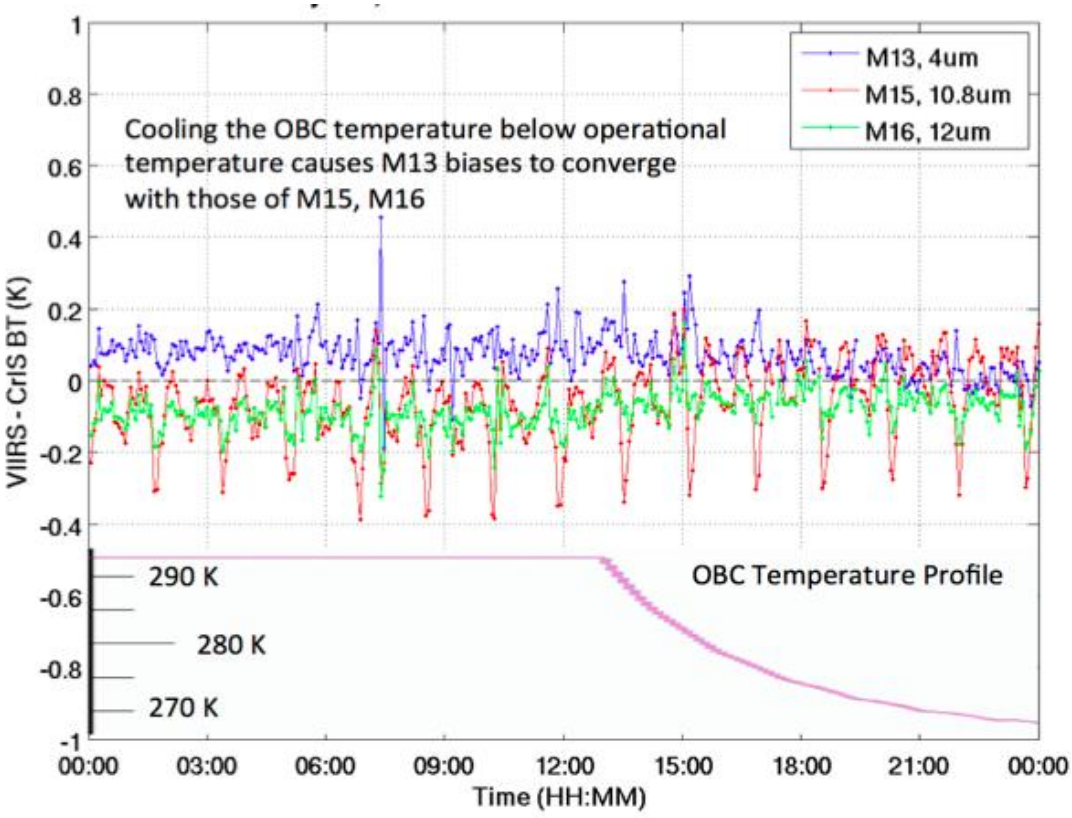

Figure 3.6. CrIS/VIIRS differences and the VIIRS OBC temperature as a function of time during a VIIRS nonlinearity characterization test.

5. IASI/VIIRS Intercalibration Results

Comparisons of Suomi-NPP VIIRS thermal emissive band SDR radiances to those of Metop-5 IASI are revealing VIIRS on-orbit calibration performance. The comparisons are based upon simultaneous nadir observations (SNOs) using a 10 minute tolerance on the temporal co-incidence of the SNPP and Metop-5 satellites. From late March through mid-October 2012, approximately 1000 good quality SNOs have been collected and processed. Each SNO is a comparison of all VIIRS and IASI footprints falling with 50 km radius of the SNO point. VIIRS spectral response information is used to convert the IASI high spectral resolution data into a VIIRS-equivalent broad band measurement.

VIIRS-IASI comparisons have revealed important TEB performance characteristics:

1. VIIRS LWIR bands M14-M15, I5 agree closely (< 0.1K) with IASI for typical earth scene temperatures (Fig CCM1), indicating excellent performance accuracy. At very cold scenes, the differences become larger, possibly indicating a need for adjusting the VIIRS offset calibration coefficient of these bands.
2. MWIR band M13 also agrees closely (< 0.2 K) with IASI for typical earth scene temperatures. However, for cold scenes (<240 K) the difference increases rapidly to more than 1 K, again meriting review of the VIIRS offset calibration coefficient.
3. A similar pattern is seen for MWIR bands M12 and I4; however, M12 and I4 show a much larger offset at typical scene temperatures than does M13. This is an artifact of incomplete spectral coverage of M12 and I4 by the IASI instrument. Tests indicate that a correction for incomplete spectral coverage will bring VIIRS into the same close agreement exhibited by band M13 for typical earth scene temperatures. At cold scenes, bands M12 and I4 also exhibit a rapidly increasing difference with IASI, similar to that shown by M13.
4. VIIRS Out-of-Band spectral response contribution to the VIIRS integrated signal is found to be small as evidenced by comparisons with IASI using the full VIIRS RSR (in-band + out-of-band regions) and using in-band only spectral region (Fig CCM2). The largest contributions (M13 and M15) are < 0.1 K.

VIIRS-IASI difference data sample is not sufficient at this time to observe meaningful trends over time in VIIRS performance. The 1st year of data comparisons will be completed at the end of the 1st quarter 2013 and will be reviewed for any indication of seasonal dependencies in VIIRS TEB calibration.

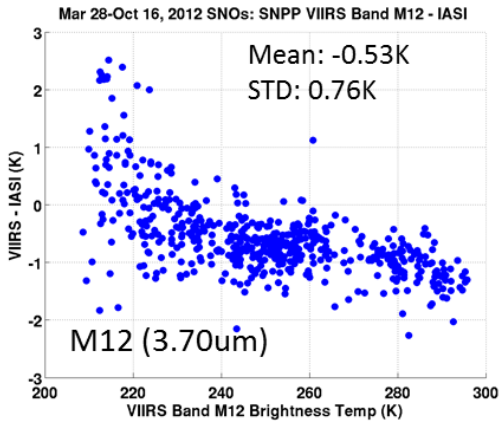

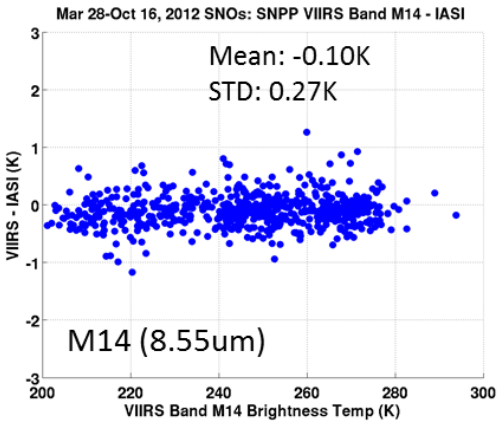

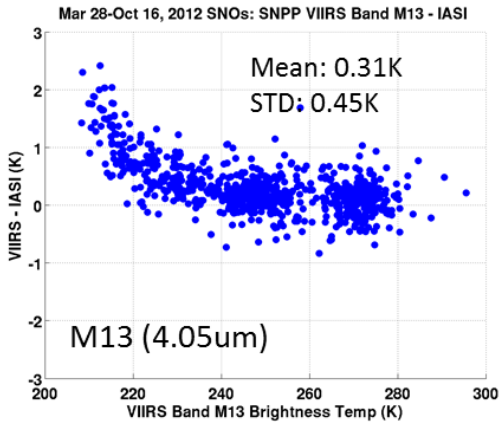

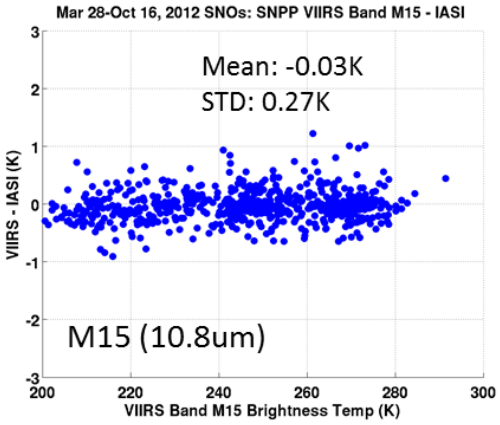

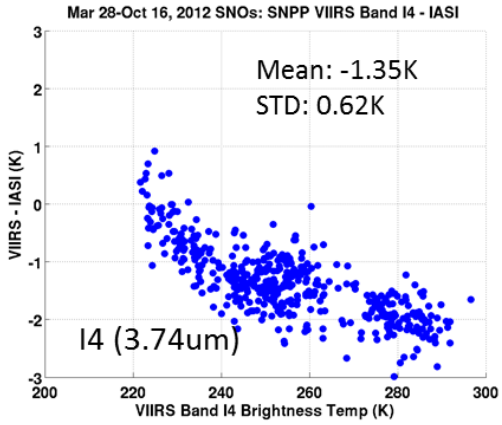

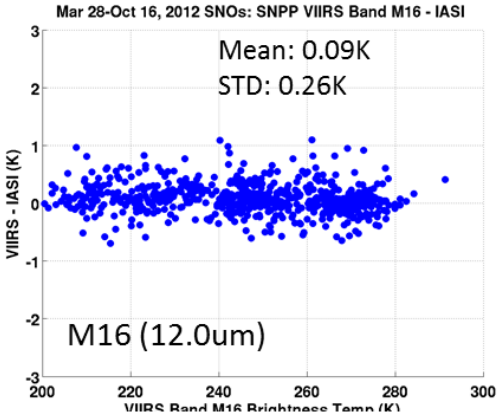

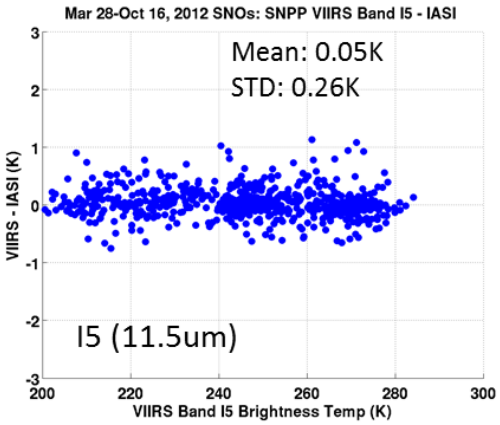

Figure CCM1. VIIRS – IASI differences for all VIIRS TEB.

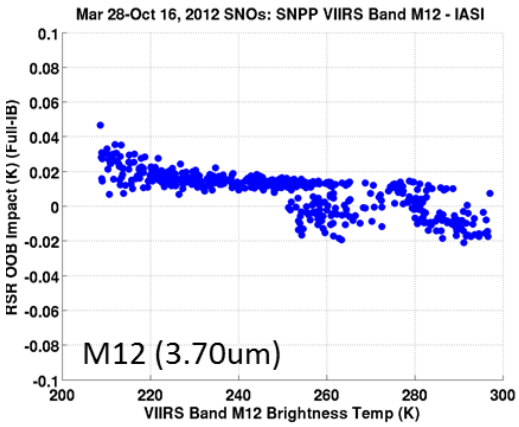

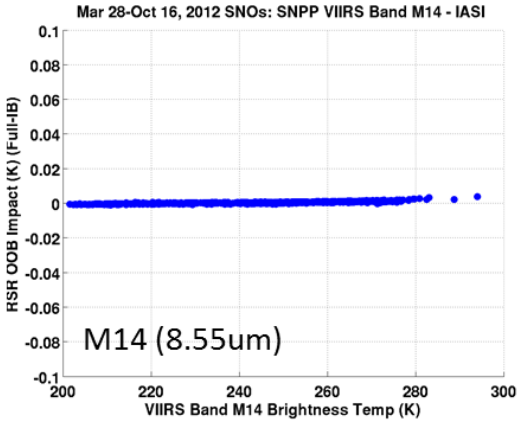

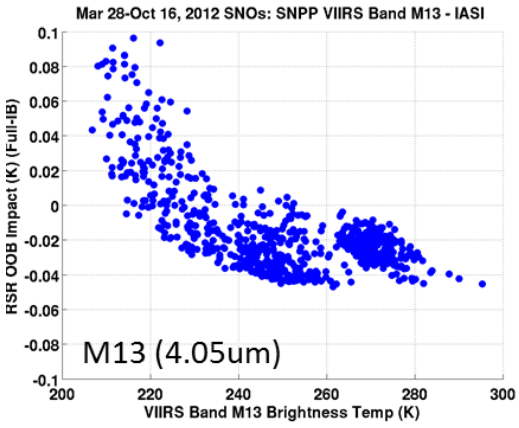

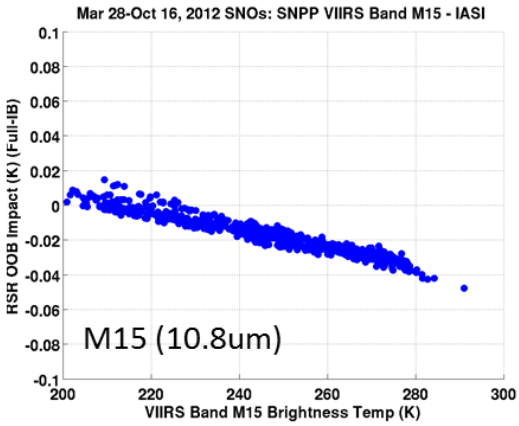

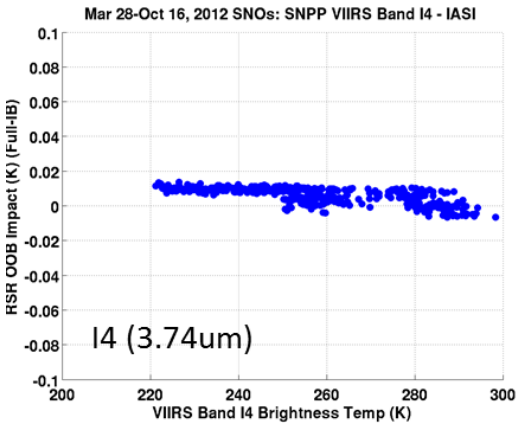

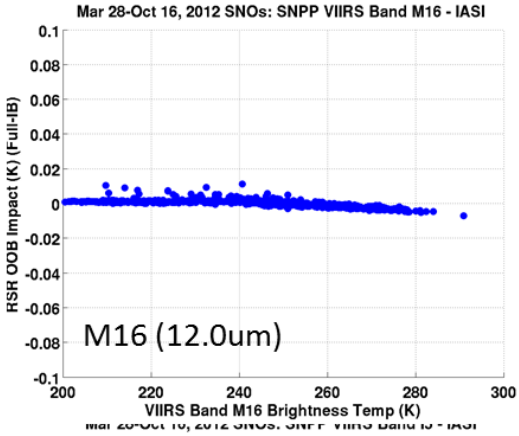

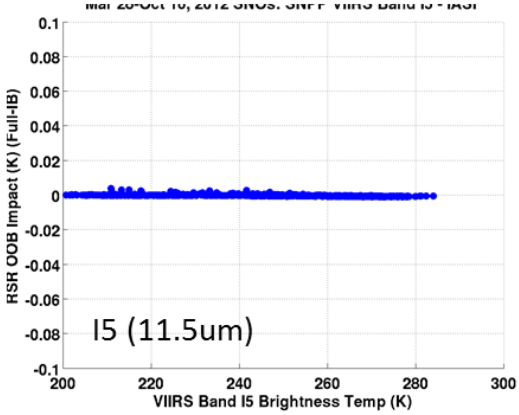

Figure CCM2. VIIRS out–of-band radiometric contribution simulated using IASI observations.